Filament Poisoning at Typical Carbon Nanotube Deposition Conditions by Hot-Wire CVD

C. J. Oliphant[1,2], C. J. Arendse[1,*], G. F. Malgas[1], D. E. Motaung[1,2], T. F. G. Muller[2], B. A. Julies[2] and D. Knoesen[2]

[1] National Centre for Nano-Structured Materials, CSIR Materials Science and Manufacturing, P. O. Box 395, Pretoria 0001, South Africa

[2] Department of Physics, University of the Western Cape, Private Bag X17, Bellville 7535, South Africa

Abstract

We report on the poisoning of tungsten filaments during the hot-wire chemical vapour deposition process at typical carbon nanotube deposition conditions and filament temperatures ranging from 1400 – 2000 °C. The morphological and structural changes of the filaments were investigated using scanning electron microscopy and x-ray diffraction, respectively. Our results conclusively show that the W-filament is not stable during the carburization process and that both mono- and ditungsten-carbides form within the first 5 minutes. Cracks and graphitic microspheres form on the carbide layer during the first 15 minutes at temperatures ≥ 1600 ℃. The microspheres subsequently coalesce to form a graphite layer, encapsulating a fully carburized filament at 2000 °C after 60 minutes, which inhibits the catalytic

[*] Corresponding author: C. J. Arendse (CArendse01@gmail.com)
Tel: +27 12 841 3671, Fax: +27 12 841 2229

activity of the filament to produce atomic hydrogen. The structural changes of the filament also induce variations in its temperature, illustrating the instability of the filament during the deposition of carbon nanotubes.

Keywords

Carburization, filament poisoning, carbon nanotubes, hot-wire CVD, instability

1. Introduction

The hot-wire chemical vapour deposition (HWCVD) process has been extensively used for the deposition of various materials, including diamond [1], polymers [2], silicon thin films [3], boron-carbon-nitride layers [4] and carbon nanotubes (CNTs) [5]. The process relies on the catalytic decomposition of precursor gases into reactive gaseous species by a resistively heated filament. A variety of transition metals, such as tungsten (W), tantalum (Ta) and rhenium (Re), have been utilised as the filament during the HWCVD process [6, 7]. This is primarily due to their high melting points and superior mechanical stabilities at temperatures above 1500 °C. Furthermore, different filaments have different abilities to dissociate the precursors. For example, a Ta filament dissociates molecular hydrogen (H_2) into atomic hydrogen (H^o) twice as efficient as a W filament during the deposition of microcrystalline silicon thin films [6].

Reactions between the precursor gases and the heated filament result in changes of the structural properties of the filaments; a process referred to as

filament ageing. The most comprehensive study on the filament ageing process in a methane atmosphere, hereafter referred to as filament carburization, was executed for the synthesis of diamond [1, 7, 8-13]. Filament carburization has several implications for HWCVD; of which the most notable is that the catalytic ability of the filament changes during carburization, since the structure and the temperature of the filament vary during the deposition [6], which consequently results in unstable deposition conditions. Furthermore, from a manufacturing point of view, carbides are brittle materials and therefore the formation thereof reduces the lifetime of the filament.

The structure and properties of CNTs deposited by HWCVD are a direct consequence of the deposition parameters, such as the growth temperature, deposition pressure, gas mixtures and flow rates. These effects are usually reported in literature [5, 15, 16], with the assumption that the structure and temperature of the filament remain stable during deposition. We therefore report on the stability of the morphology, structure and temperature of the W-filament at typical CNT deposition conditions [5, 15, 16], probed as a function of exposure time and filament temperature, using scanning electron microscopy (SEM), x-ray diffraction (XRD) and in-situ temperature measurements, respectively. Furthermore, the morphology of the resultant CNTs will be compared and related to the structural changes of the filament for different filament temperatures.

2. Experimental

2.1 The filaments

Coiled W-filaments (99.95 % purity) of length 350 mm and diameter 0.5 mm were carburized in a quartz tube HWCVD reactor [16], using a CH_4:H_2 atmosphere of 1:10 at a deposition pressure of 150 Torr. The filaments were resistively heated to its desired temperature by a 1 kW DC power supply and its temperature was measured using a two-colour optical pyrometer (Raytek® Marathon MR1S series, 0.75% error), located ~1.5 m away from the filament. Exposure times amounted to 5, 15 and 60 minutes at temperatures ranging from 1400 – 2000 ℃, in increments of 200 ℃. The t emperature of the filament was monitored in-situ as a function of time during carburization with a resolution of 1 minute. After carburization the filaments were allowed to cool down to room temperature in vacuum, after which they were removed and then stored away for analysis. The filaments were highly brittle after the carburization and therefore great care was taken when removing the filaments in order to prevent any mechanical disturbance to its surface.

2.2 Characterization

Cross-sections of the carburized filaments were prepared by grinding and subsequent polishing using diamond lapping films. The surface and cross-sections of the W-filaments were examined using a Hitachi X-650 SEM operated at 12 – 25 kV and equipped with a semiconductor detector that allows for the detection of energy dispersive x-rays (EDX). The morphology of the carbon nanotubes were characterized using a LEO 1525 field emission

scanning electron microscope (FESEM) operated at 3 – 10 kV. Phase identification, performed on a coil from the central part of the filament, was measured using the Phillips PW 1830 x-ray powder diffractometer in a $\theta - 2\theta$ geometry, operated at 45 kV and 40 mA. The XRD spectra were collected at 2θ-values ranging from 10 – 80° with a step size of 0.02°. Copper $K\alpha_1$ radiation with a wavelength of 1.5406 Å was used as the x-ray source. The tungsten, tungsten-carbide and graphite phases were identified using the diffraction pattern database maintained by the Joint Committee for Powder Diffraction Studies (JCPDS) [17].

3. Results and Discussion

Fig.1 shows an SEM micrograph of an industrially pure W-filament and its XRD spectrum (insert) as reference. Three characteristic XRD peaks are evident which are associated with the tungsten body centred cubic (bcc) crystal structure. The surface of the filament has grooves indicating that it was produced by an extrusion method. Furthermore, the surface is covered with carbonaceous impurities which confirm the need to heat the filament prior to deposition in order to remove any impurities from its surface.

The SEM micrographs of the centre sections of filaments operated at 1400 °C for 5 and 15 minutes are depicted in Fig. 2. The filament shows minimal morphological changes. However, XRD reveals that the filament-surface has carburized to ditungsten carbide (W_2C) and monotungsten carbide (WC) during the first 5 minutes (Fig. 3). Subsequently, the WC phase dominates after 15 minutes, as suggested by the increase in its XRD

intensities relative to the W_2C and the W phases. The appearance of the WC phase is more rapid than previously reported for diamond synthesis [10] and is attributed to the higher CH_4 concentration and deposition pressure used.

Operating the W-filament at 1600 ℃ for 5 minutes, results in the deposition of hemispherical deposits, of diameter ~ 35 μm, which are carbonaceous according to EDX analysis (see Fig. 4a and b). The formation of these carbon deposits, referred to as carbon microspheres, have been reported recently [18] and its growth mechanism involves the adsorption of hydrocarbon species onto the filament surface followed by the formation of tungsten carbide microspheres which act as nucleation centres for the growth of carbon microspheres. XRD analysis (Fig. 4c) confirms, from emergence of the diffraction peak at $2\theta \sim 26°$, that the microspheres are graphitic. The graphitic microspheres eventually become more densely packed as the exposure time increases and appear to be growing preferentially along the grooves of the filament, ultimately resulting in an encapsulating layer after 60 minutes of exposure, as shown in Fig. 4d.

The temperature dependence of the carburization process becomes more apparent when increasing the temperature to 1800 ℃. Fig. 5 reveals that cracks form along the length of the filament after 5 minutes and that the graphitic microspheres only appear on the surface after 15 minutes. The filament crystals re-aligned themselves perpendicular to the filament-axis during carburization, as illustrated in the insert of Fig. 5a. This is indicative of a diffusion based growth, which is characteristic for carburization [1].

Fig. 6a shows that the graphitic microspheres initially grow inside the cracks of the filament after 15 minutes when increasing the temperature to 2000 ℃. Prolonged exposure of the filament for 60 minutes again results in the encapsulation of the filament with a thicker solid graphitic layer as compared to 1600 °C, as shown in Fig. 6b. Cross-sections of the carburized W-filament operated at 2000 °C for 15 and 60 minutes were prepared to observe the transformation of its internal structure (see Fig. 6c-d). After 15 minutes, the central core of the filament corresponds to pure W, while the surface displays cracks which are indicative of a carbide region as deduced from the XRD analysis. After 60 minutes of carburization the filament-diameter increase to approximately 600 μm and is covered by a solid graphite layer, approximately 180 μm thick, that is composed of sheets. Moreover, the cracks extend through the entire filament, indicating a fully carburized filament [1, 10].

The distinguishable feature of HWCVD over its thermal counterpart is its inherent characteristic to generate copious concentrations of atomic hydrogen via the catalytic dissociation of H_2 into atomic hydrogen by the heated W-filaments [14, 19]. This characteristic is especially beneficial to the deposition of CNTs, since atomic hydrogen etches amorphous carbon bonds and prevents the deposition of encapsulating carbon layers on the catalysts particles, thereby maintaining their activity [20]. However, the formation of solid graphitic layers on the filament-surface has shown to inhibit the catalytic ability of the filament to produce atomic hydrogen and has been consequently

referred to as filament poisoning [14]. The results presented in this study therefore suggest that operating W-filaments at temperatures above 1600 ℃ is not desirable as filament poisoning occurs within the first 5 minutes of deposition, which is be detrimental to the growth of CNTs with high purity.

The structural changes of the filament is clearly demonstrated by its effect on the temperature, as illustrated in Fig. 7 where the evolution of the filament temperature is plotted as a function of time for initial temperatures of 1400 °C and 2000 °C. The increase in the filament-temperature during the first 5 minutes is attributed to the appearance of the W_2C and WC phases, which have higher resistivities than W. At 1400 ℃ the temperature gradually starts to decrease after 5 minutes' exposure to its initial value after 60 minutes. This is due to the enhancement of the WC phase, which has a lower resistivity than W_2C. In contrast, at 2000 ℃ the graphite layer becom es thicker with increased exposure times, resulting in an increased filament-diameter. This observation in conjunction with the higher emissivity of graphite (~0.9), result in a rapid decrease of the temperature to a final value of ~ 1700 °C after 60 minutes.

Thus far, this contribution suggests 1400 °C as the optimum filament temperature for the deposition of CNTs at the deposition conditions described. As a preliminary comparative investigation, CNTs were synthesized on a $Ni/SiO_2/Si$ substrate at a filament temperature of 1400 and 1600 °C for a deposition time of 15 minutes, where the required nano-sized Ni-islands were prepared by annealing the substrate at 500 °C for 20 minutes in a 100 sccm

H_2 flow at a pressure of 30 mTorr. Fig. 8 shows an atomic force microscopy (AFM) topograph of the substrate after annealing, which confirms the formation of Ni islands of diameters ranging from 50 – 200 nm. The SEM micrographs, depicted in Fig. 9, demonstrate that straight multi-walled CNTs with minimal defects and a low degree of buckling are observed for a filament temperature of 1400 °C. The MWCNTs deposited at 1600 °C are more entangled with a high degree of surface coverage by amorphous carbon. The increased defect density at 1600 °C is attributed to the decrease in the concentration of atomic hydrogen during deposition, caused by the onset of filament poisoning by formation of the graphitic microspheres on the W-filament.

4. Conclusion

The results demonstrate that the structure, morphology and temperature of the W-filament are not stable during typical CNT deposition conditions. SEM and XRD reveal that both WC and W_2C phases nucleate on the surface of the filament after 5 minutes at temperatures ≥ 1400 °C. At temperatures ≥ 1600 °C, graphitic microspheres and cracks form along the length of the filament after 5 minutes. The microspheres eventually grow in size and density to eventually encapsulate the filament after 60 minutes, which inhibits the filament's ability to produce atomic hydrogen that result in defect-rich CNTs. Furthermore, in-situ temperature measurements reveal that the encapsulation process induce a temperature drop of ~ 300 °C.

Acknowledgements

The authors acknowledge the financial support of the Department of Science and Technology of South Africa and the CSIR (Project no: HGERA2S). The authors are especially thankful to Mr Adrian Josephs (Microscopy Unit, University of the Western Cape) for his assistance with the SEM measurements and sample preparation.

References

[1] T. D. Moustakas, Solid State Ionics 32-33 (1989) 861

[2] A.C. Rastogi and S.B. Desu, Polymer 46 (2005) 3440

[3] S.A. Filonovich, M. Ribeiro, A.G. Rolo and P. Alpuim, Thin Solid Films 516 (2008) 576

[4] R. Weissenbacher, R. Haubner, K. Aigner and B. Lux, Diam. Rel. Mater. 11 (2002) 191

[5] A.C. Dillon, A.H. Mahan, J. L. Alleman, M. J. Heben, P.A. Parilla and K.M. Jones, Thin Solid Films 430 (2003) 292

[6] M. Sommer and F. W. Smith, J. Mater. Res. 511 (1990) 2433

[7] C. H. M. van der Werf, P. A. T. T. van Veenendaal, M. K. van Veen, A. J. Hardeman, M. Y. S. Rusche, J. K. Rath and R. E. I. Schropp, Thin Solid Films 430 (2003) 46

[8] A. Kromka, J. Janík, A. Šatka, J. Pavlov and I. Červeň, Acta Physica Slovaca 51 (2001) 359

[9] M. Sommer, K. Mui and F. W. Smith, Solid State Communications 69 (1989) 775

[10] S. Schwarz, E. Zeiler, S. M. Rosiwal and R. F. Singer, Materials Science and Engineering A 335 (2002) 236

[11] S. Okoli, R. Haubner and B. Lux, Surface and Coatings Technology 47 (1991) 585

[12] H. Matsubara and T. Sakuma, Journal of Material Science 25 (1990) 4472

[13] C. F. Davidson, G. B. Alexander and M. E. Wadsworth, Metallurgical Transactions A 10A (1979) 1059

[14] R. Hernberg, D. M. Li and T Mäntylä, Diamond and Related Materials 7 (1998) 1709

[15] C. Wolden and K. K. Gleason, J. Appl. Phys. 62 (1994) 3102

[16] C. J. Arendse, G. F. Malgas, M. R. Scriba, F. R. Cummings and D. Knoesen, Journal of Nanoscience and Nanotechnology 7 (2007) 1

[17] Joint Committee for Powder Diffraction Studies (JCPDS): W (89-3012), W_2C (79-0743), WC (89-2727) and graphite (75-1621)

[18] S. M. C. Vieira, C. A. Rego and P. R. Birkett, Diam. Rel. Mater. 17 (2008) 100

[19] L. Langmuir, J. Am. Chem. Soc. 34 (1912) 1310

[20] S. Honda, M. Katayama, K. Lee, T. Ikuno, S. Ohkura, K. Oura, H. Furuta and T. Hirao, Japanese Journal of Applied Physics 42 (2003) L441

List of Figure Captions

Fig. 1 SEM micrograph of an industrially pure W-filament and its XRD spectrum (insert)

Fig. 2 SEM micrographs of the filament-surface operated at 1400 ℃ for (a) 5 minutes and (b) 15 minutes

Fig. 3 XRD spectra of the filament-surface operated at 1400 ℃ for 5 and 15 minutes

Fig 4 (a) SEM micrograph of the filament-surface operated at 1600 ℃ for 5 minutes

(b) EDX spectrum of the globule shown in the inset of (a)

(c) XRD spectra of the filament-surface operated at 1600 ℃ for 5 minutes

(d) SEM micrograph of the filament-surface operated at 1600 ℃ for 60 minutes

Fig. 5 SEM micrographs of the filament-surface operated at 1800 ℃ for (a) 5 minutes and (b) 15 minutes. The insert in (a) is at a higher magnification

Fig. 6 SEM micrographs of the filament-surface operated at 2000 ℃ for (a) 15 minutes and (b) 60 minutes and of the cross-sections of the

filament operated at 2000 ℃ for (c) 15 minutes and (d) 60 minutes

Fig. 7 Filament temperature as a function of exposure time for initial temperatures of (a) 1400 °C and (b) 2000 °C

Fig. 8 AFM topograph of the Ni/SiO_2/Si substrate after annealing

Fig. 9 SEM micrographs of MWCNTs deposited at a filament temperature of (a) 1400 °C and (b) 1600 °C

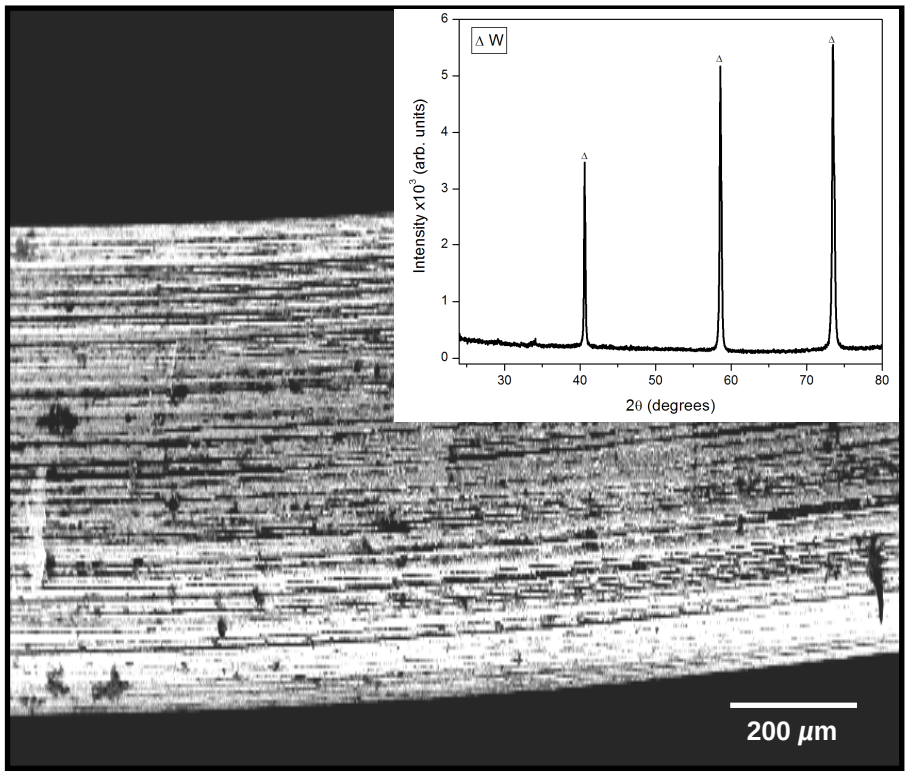

Figure 1 (Oliphant et al)

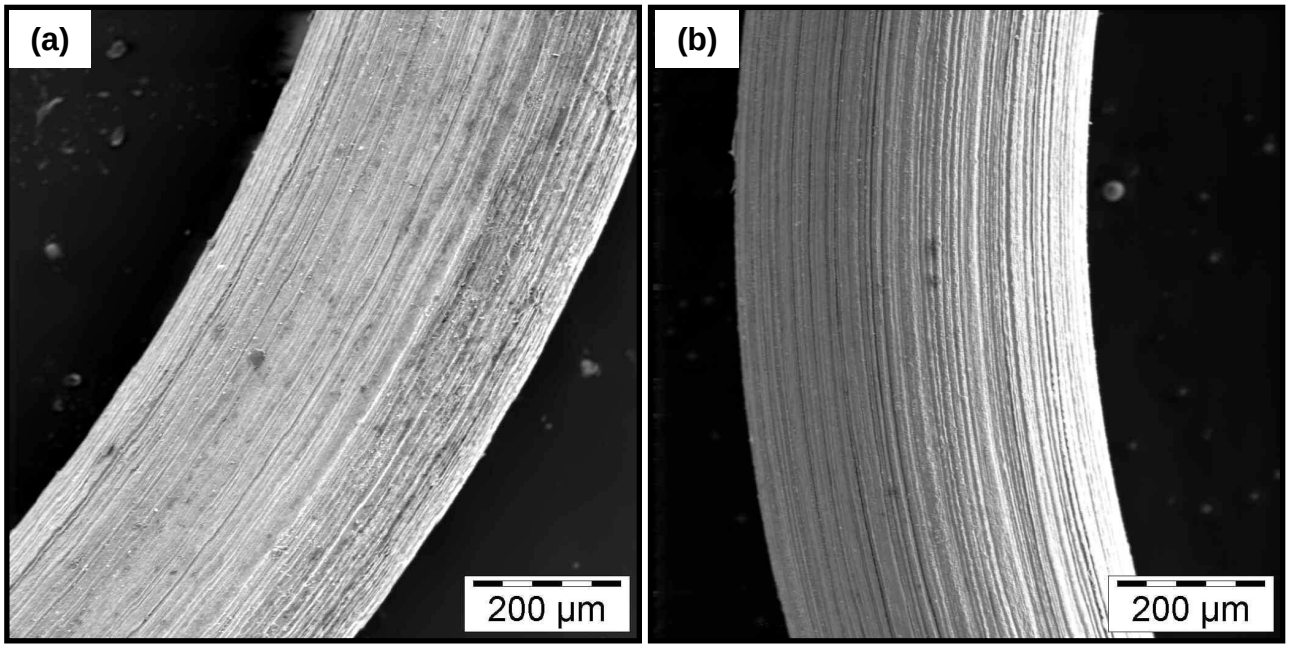

Figure 2 (Oliphant et al)

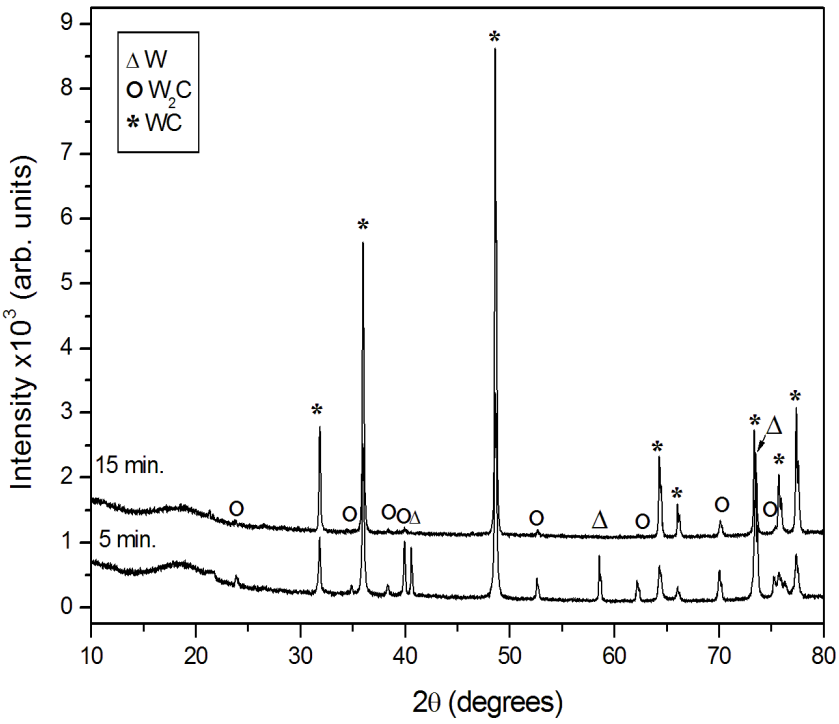

Figure 3 (Oliphant et al)

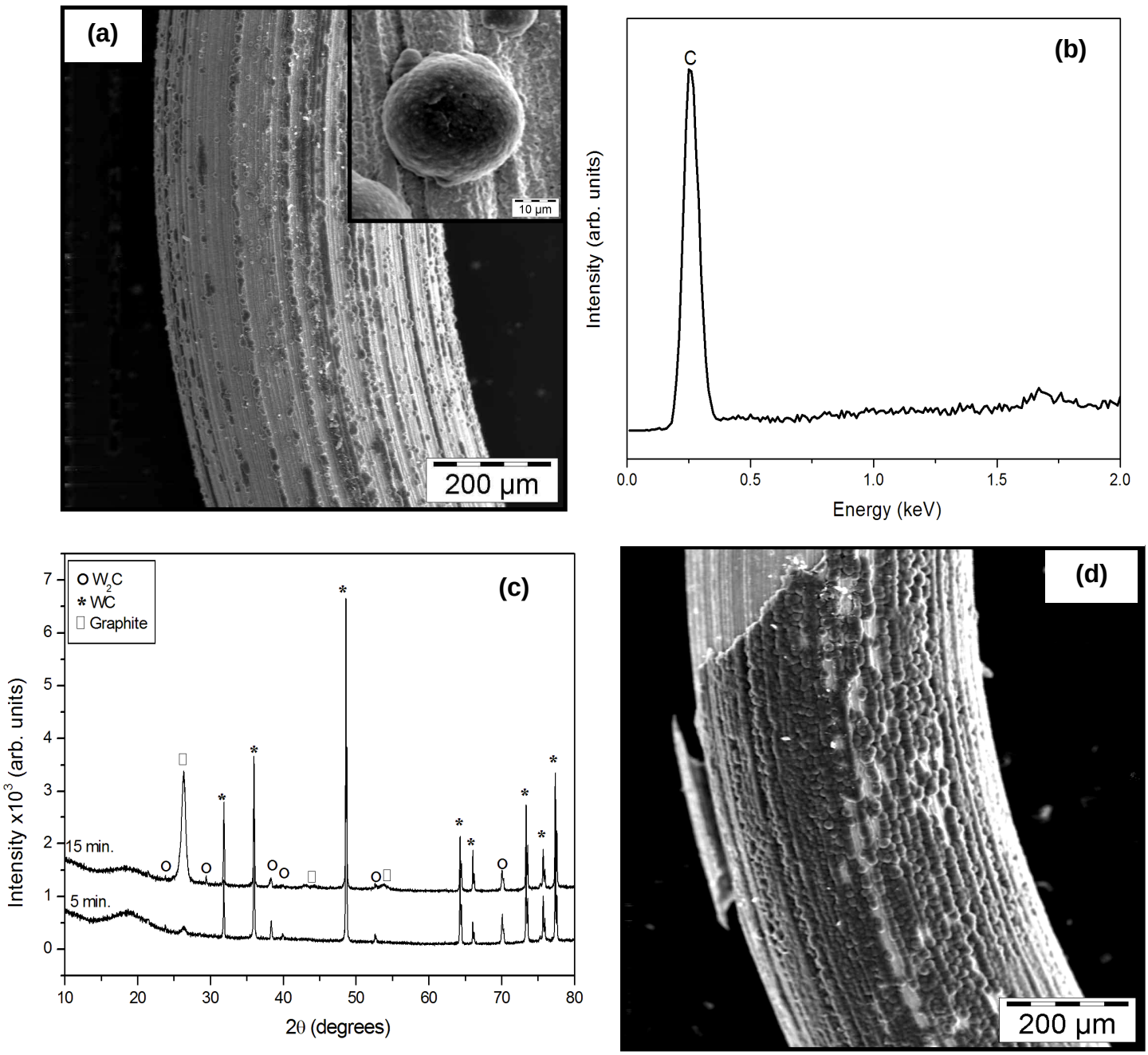

Figure 4 (Oliphant et al)

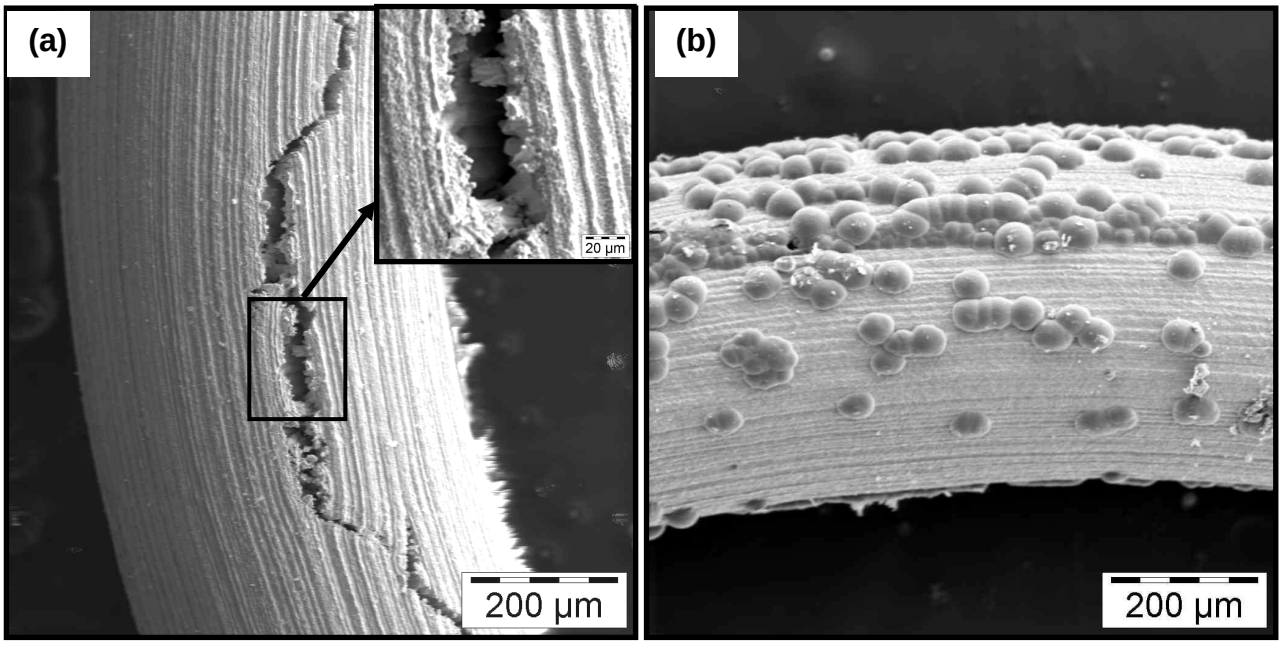

Figure 5 (Oliphant et al)

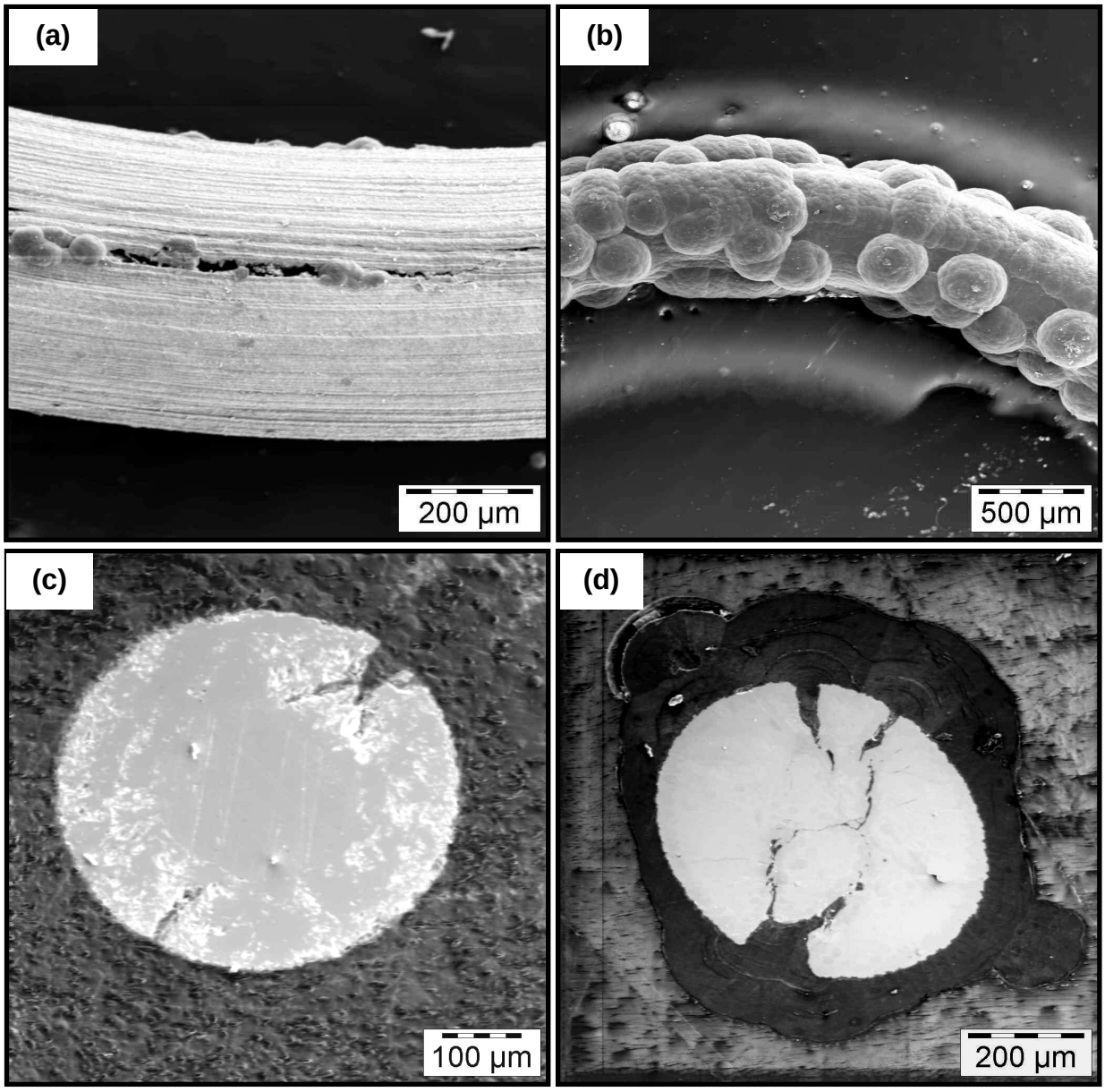

Figure 6 (Oliphant et al)

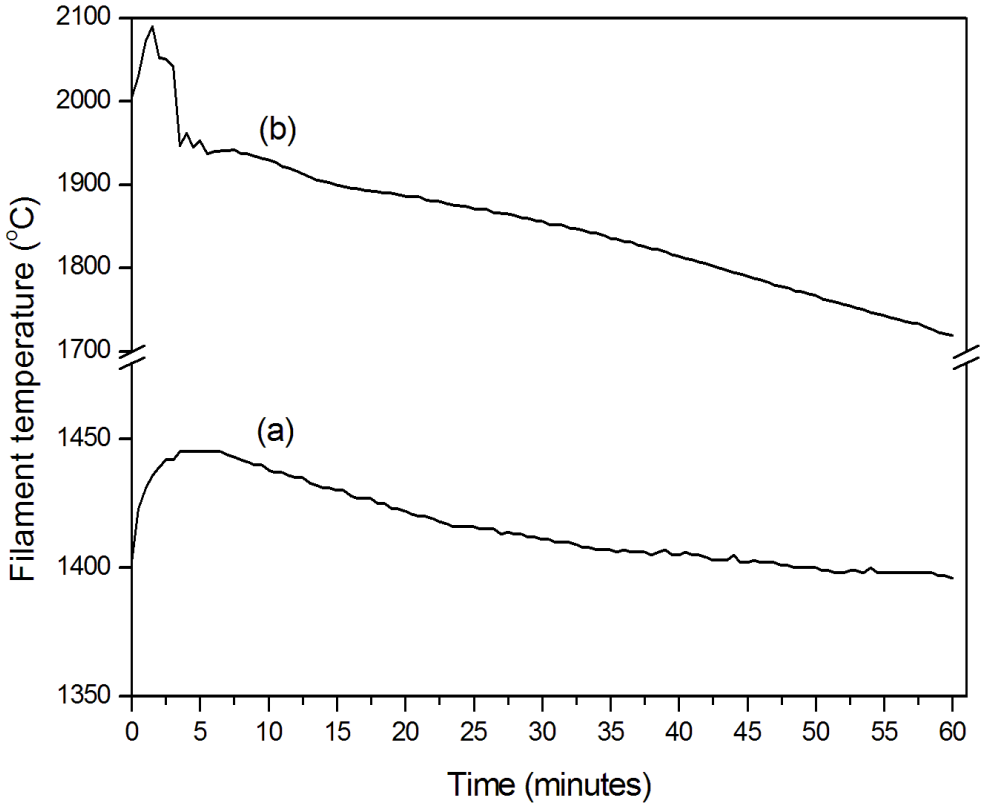

Figure 7 (Oliphant et al)

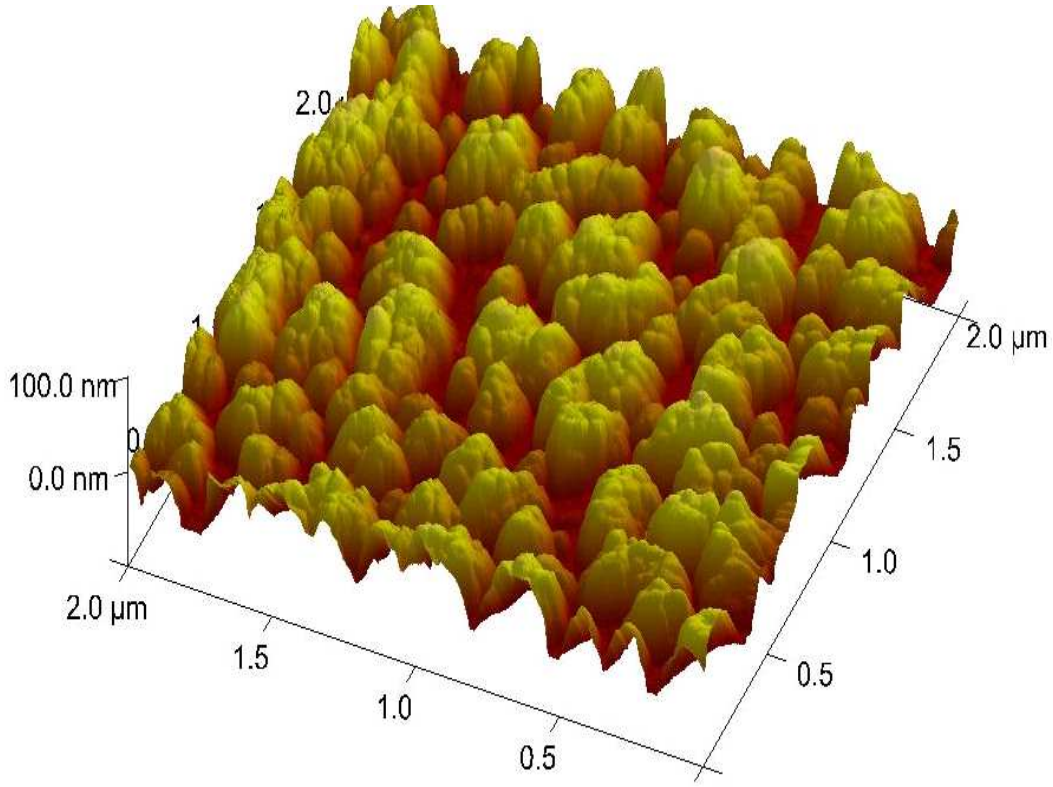

Figure 8 (Oliphant et al)

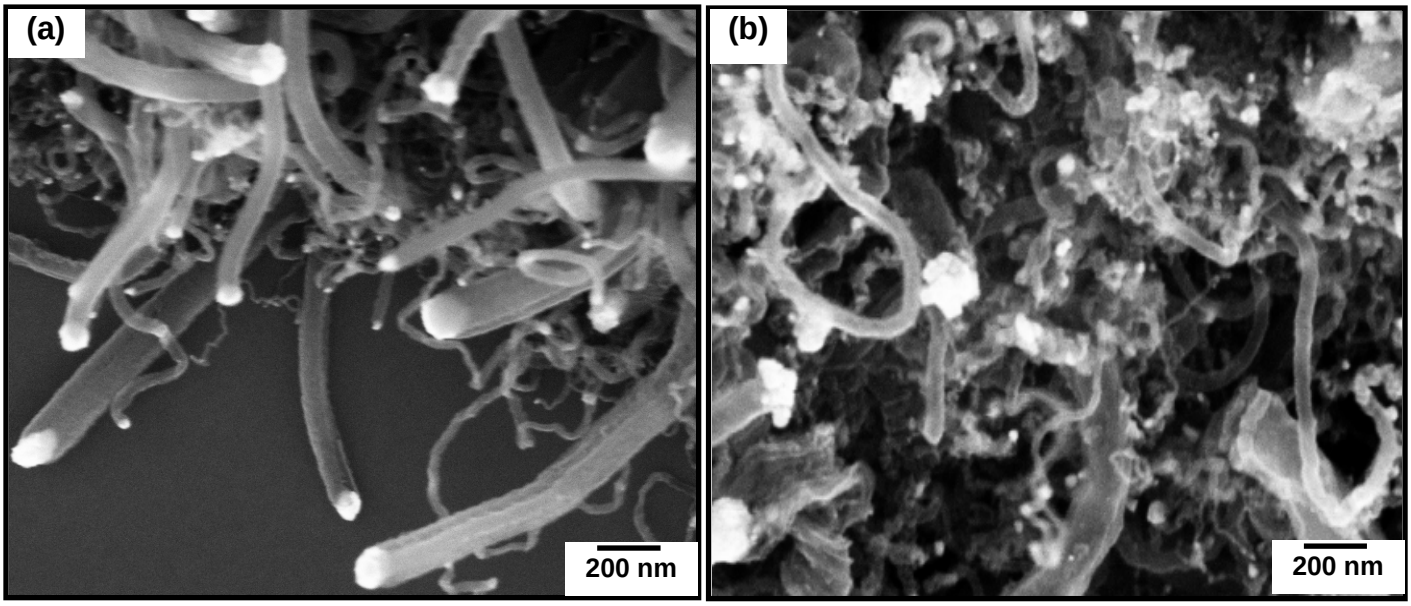

Figure 9 (Oliphant et al)